Hindawi
Structural Control and Health Monitoring
Volume 2023, Article ID 6061653, 10 pages
https://doi.org/10.1155/2023/6061653

Research Article

Fabrication of Microcapsule-Type Long-Lasting Phosphorescent Sensor for Concrete Crack Monitoring

Yayun Zhao,[1] Yao Li,[1] Qing Wang ,[1,2,3] and Haohui Zhang[1]

[1]*College of Civil Engineering and Architecture, Shandong University of Science and Technology, Qingdao, 266590 Shandong, China*
[2]*College of Mechanical and Architectural Engineering, Taishan University, Tai'an, 271000 Shandong, China*
[3]*Institute of Advanced Engineering Materials and Structures, Taishan University, Tai'an, 271000 Shandong, China*

Correspondence should be addressed to Qing Wang; qwang@sdust.edu.cn

Received 28 December 2022; Revised 8 August 2023; Accepted 21 August 2023; Published 9 September 2023

Academic Editor: Young-Jin Cha

The generation and expansion of cracks in concrete structures reduce the durability and safety of structures. In order to detect cracks in concrete structures, a long-lasting phosphorescent microcapsule coating is proposed in this study. The microcapsule-based sensor is pasted on the surface of cement-based materials and solidified. The microcapsules become ruptured and cause the core material to flow out when the microcracks occur on the material, which emits strong phosphorescence at the cracked position under UV irradiation. The results indicate that the successful encapsulation of microcapsules could enhance the thermal stability of phosphorescent dye. The excitation wavelength of the phosphorescent microcapsules is also investigated. The phosphorescent microcapsules could effectively highlight unnoticeable cracks by a long-lasting phosphorescence response in the cracking region. The mechanical properties of microcapsules/epoxy resin composite coatings were studied, and the optimal content of microcapsules in the coating was determined. The as-fabricated phosphorescent microcapsules have good damage-sensing effects in conditions of different light and temperatures. The method proposed in this study will assist in the further development of damage-sensing material in the field of concrete crack monitoring.

1. Introduction

Concrete materials are widely used for structure construction because of their high strength, low cost, corrosion resistance, and simple construction process. However, due to the brittleness nature and external loading, cracking is a common phenomenon in concrete structures. The generation and propagation of microcracks may cause corrosion of steel bars and carbonization of concrete and reduce the durability of structures. The excessive development of cracks will reduce the bearing capacity and even shorten the service lifespan of the structure [1]. The monitoring of concrete cracks is of great significance for damage diagnosis, structural maintenance, and component repairing [2]. At present, a series of damage monitoring methods based on electronic sensors for concrete crack monitoring have been reported [3, 4]. Distributed optical fiber sensors [5–7], piezoelectric sensors [8–11], flexible strain sensors [12], and acoustic emission sensors [13] were developed for structural health monitoring. These traditional sensors are extremely dependent on external power supply and data-processing equipment. Moreover, the application methods of traditional sensors are complex, which brings inconvenience to their application in many scenarios [14].

Novel smart sensing materials provide simple and fast approaches to the preliminary detection of structural cracks [15, 16]. Mechanochromic photonic crystals [17, 18], as visual sensors, were extensively studied due to their regular color variation under different viewing angles and external force conditions. However, the complicated preparation process and the influence of observation angle on structural color are the main problems limiting photonic crystals' application. Dye-filled hollow fibers [19, 20] have been developed to achieve targeted damage detection and local

self-repair, while the fiber dimension makes it unable to adapt to complex structure forms. Advanced microcapsule-based materials can solve these problems well. Due to their micro nanoscale, microcapsules can be flexibly applied to various complex surfaces [21, 22]. Microcapsules containing sensing coatings were designed to report damage via color reaction of core material and injury site [23] or inducer [24–26] after the microcapsules ruptured. Fluorescent microcapsules were also proposed for damage sensing [27–29]. However, the fluorescent material only has a nanosecond fluorescence lifetime [30], which requires continuous excitation when observing damage. Besides, the excitation light source will interfere with the observation to a certain extent. Thus, the trigger principles of previous studies are restricted, or the expression performances need to be more obvious for structural health monitoring. Furthermore, complex preparation processes and expensive inducers are often required to achieve mechanochromic function in the damage-detecting system. Long-lasting phosphorescent materials were reported to have long-lasting characteristics, and obvious luminescence after the excitation light was removed [31, 32]. This provides new approaches for the design of damage-sensing materials.

A long-lasting phosphorescent microcapsule coating is proposed to detect cracks in concrete structures in this study. The solvent evaporation method was used to fabricate the microcapsule-type long-lasting phosphorescent sensing material for concrete crack monitoring. The prepared microcapsules can be pasted on the surface of cement-based materials and solidified. As shown in Figure 1, the synthesized phosphorescent microcapsules were added to epoxy resin E-51 to prepare a crack-sensing coating. The coating was directly brushed into the structure. Because the microcapsule shell is transparent, a layer of epoxy is applied to the cured coating to block UV to avoid the influence of microcapsule auto-luminescence on monitoring results. The microcapsules will be ruptured and cause the core material to flow out when the microcracks occur on the material, which emits strong phosphorescence at the cracked position under UV irradiation. Regular spherical microcapsules could be obtained under 500–1100 rpm stirring, and the thermal gravimetric analysis results indicated that microencapsulation could enhance the stability of core material. The application test showed that the as-fabricated microcapsules had noticeable crack-sensing performance under different light conditions and temperatures. After removing the excitation light source, the phosphorescent microcapsule could still provide more than 10 min phosphorescence for damage observation, which can effectively avoid the interference of the excitation light source and reduce the difficulty of crack observation.

2. Materials and Methods

2.1. Materials. Dichloromethane (AR) and polymethyl methacrylate (PMMA, 100 mesh) were purchased from Zhong Xin Plastic (China). Oily long-lasting phosphorescent dye and isoamyl acetate were obtained from Foshan XiuCai Chemical Co., Ltd. (China). Polyvinyl alcohol (PVA, 17–88, 160 meshes) was purchased from Usolf Chemical Technology Co., Ltd. (China). The curing agent (593) and epoxy resin (E-51) were purchased from China Petrochemical Corporation.

2.2. Fabrication of Microcapsules. Figure 2 shows the schematic representation of the microcapsule fabrication method used in this study. The phosphorescent microcapsules were synthesized by a facile solvent evaporation method with a magnetic stirrer (85-2A, JintanYoulian Instrument, China). The PVA (1.6 g) was put into deionized water (80 ml) at 80°C and stirred at 1000 rpm until completely dissolved. The temperature of the dissolved solution was decreased to 20°C as the aqueous phase. Commercial oily long-lasting phosphorescent dye (phosphorescent paint containing strontium aluminate) was selected as the phosphorescent liquid to prepare the microcapsule core. Then, 0.5 g of phosphorescent liquid was diluted by 2.0 g of isoamyl acetate as core material. 1 g of PMMA and 30 g of dichloromethane were mixed and stirred to dissolve and then mixed with the phosphorescent liquid as the oil phase. The aqueous and oil phases were mixed to obtain a mixed system. The mixing system was stirred at 1300 rpm for 5 minutes. And then, it was heated to 35°C and kept for 4 hours. Finally, it was stirred at 55°C for 1 hour to completely evaporate the dichloromethane to obtain the microcapsule dispersion. The microcapsule dispersion was rinsed 6 times with deionized water. Then, it was dried at 50°C for 6 hours to obtain the dry microcapsules. The mortar test block used as the base was made according to a ratio of cement : sand : water 1 : 1 : 0.45. The microcapsules were added at 0%, 5%, 10%, and 15% of the total mass of epoxy resin and curing agent to prepare the crack-sensing coating. The ratio of epoxy resin and curing agent was 3 : 1. It was applied on the surface of the mortar test block and cured at room temperature for 48 hours.

2.3. Surface Morphologies. The morphology and shape of the phosphorescent microcapsules were observed with a scanning electron microscope (SEM, SEM4000, China) after spray-gold treatment. The ruptured microcapsules were obtained through simple vertical pressing using the SEM sample stage. The microcapsules used for surface morphology were fabricated under 1100 rpm stirring.

2.4. Microencapsulation. The microencapsulation of the core material was investigated using an energy dispersive spectrometer (EDS) and Fourier transform infrared (FT-IR, JASCO, Japan) spectrometer. The KBr method was adopted to determine the infrared spectra. The tablets of ruptured microcapsules and microcapsule cores were prepared after fully grinding. For complete microcapsules, in order to ensure the integrity of the microcapsules, they were directly added into the ground KBr to prepare tablets. The EDS spectra of the intact microcapsule and core material were taken by the same SEM equipment used in surface morphology characterization under an accelerating voltage of 10.00 kV.

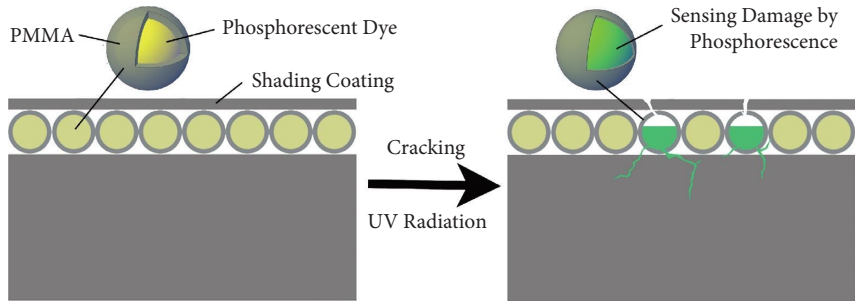

Figure 1: Schematic diagram of damage indication concept. The long-lasting phosphorescent dye is encapsulated into a polymethyl methacrylate shell. When the cracks occur and propagate on the structure surface, the microcapsules will rupture and then highlight the crack area after being exposed to UV light.

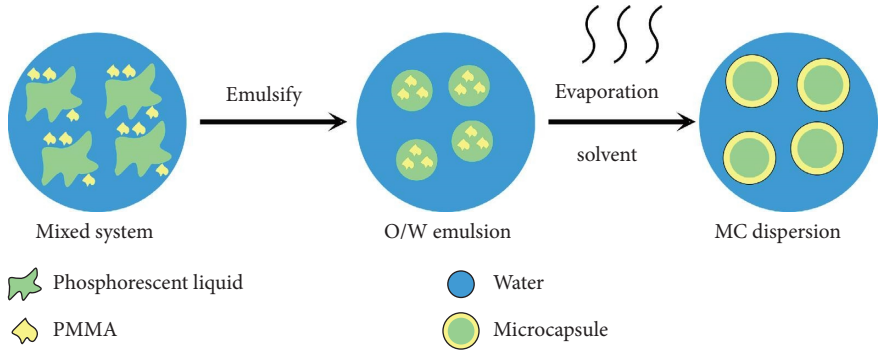

Figure 2: Preparation process of phosphorescent microcapsules.

2.5. Size Distribution of Microcapsules. A laser particle size analyzer (Rise-2006, Rise, China) was used to study the size distribution of microcapsules. Five groups of microcapsules were prepared at stirring speeds of 300 rpm, 500 rpm, 700 rpm, 900 rpm, and 1100 rpm in order to detect the particle size distribution. To prevent adhesion from affecting the results during the drying process of the microcapsules, the washed microcapsule dispersion was adopted for particle size analysis. Deionized water was used as dispersion during the experiment.

2.6. Mechanical Properties. Tensile strength tests were conducted on microcapsule/epoxy resin composite coating samples containing different microcapsule mass fractions (0.0wt%, 5.0wt%, 10wt%, and 15wt%) using a universal material testing machine (MZ-4000D). A dumbbell-shaped sample with a size of 75 mm × 4 mm × 2 mm was prepared. During the tensile testing, the microcapsule/epoxy resin composite coating sample is dragged by a 500 N force sensor at a constant speed of 2 mm/min at a temperature of 20 ± 2°C to measure the tensile breaking strength. Dynamic compression tests were conducted using a split Hopkinson pressure bar (SHPB). A cylindrical sample with a height of 6 mm and a diameter of 5.5 mm was prepared. The sample consists of microcapsule/epoxy resin composite coating with different microcapsule mass fractions to determine the compression behavior of the composite coating. To ensure statistical accuracy, three samples from each group were tested. The average of the test results is taken as the final result.

2.7. Evaluation of Phosphorescence Performance. The phosphorescent performance of dried microcapsules was tested using a fluorescence/phosphorescence spectrometer (LS-55, USA). Phosphorescence spectrum analysis was taken to measure the phosphorescence intensity of microcapsules. The excitation wavelength of microcapsules is characterized by the excitation spectrum. All spectra were measured using dried microcapsules.

2.8. Thermal Stability. The thermal stability of the phosphorescent microcapsule was evaluated by a thermogravimetric analyzer (TGA, Mettler-TGA 2, Switzerland). The heating rate was 10°C/minute from 30°C to 600°C. The thermal stability of the microcapsule phosphorescence effect was evaluated by setting the temperature at 30°C, 50°C, 70°C, 90°C, and 110°C for 12 hours in a vacuum drying oven (DHG-9623A, Jingqi, China). After each heating, the microcapsules were taken out and irradiated with a UV lamp in a dark environment to show the phosphorescent effect. Except for the marked pictures, all others were taken at room temperature.

2.9. Crack Sensing Test. A UV lamp (320 nm, 8W) was used to excite the crack area at a distance of 50 cm. A camera was used to record the crack-sensing effect. The epoxy resin, curing agent, and dried microcapsules were mixed with a mass ratio of 3 : 1 : 1 to get the crack-sensing coating mixture and then directly brushed onto the surface of mortar samples of a thickness of about 500 μm. Due to the good

transparency of PMMA, the unruptured microcapsules can also emit phosphorescence. Thus, a layer of epoxy topcoat of about 200 μm was brushed as a light-shielding coating on the surface to block UV light after the coating was completely cured. The microcapsules used in the crack-sensing test were prepared at 1100 rpm stirring. The crack-sensing effect of the same sample under different observation distances was also photographed. Limited by the video equipment, the shooting effect of the light source at the crack was quite different from the naked eye observation. Therefore, the duration of phosphorescence was measured by recording the phosphorescence duration of the whole coating without shielding coating.

3. Results and Discussion

3.1. Surface Morphologies of Microcapsules. The SEM images of phosphorescent microcapsules at different magnifications are shown in Figure 3. The microcapsules are uniformly formed and have a similar size distribution, which is mostly distributed in the range of 20 μm to 60 μm (Figure 3(a)). The phosphorescent microcapsule has a full spherical shape and a smooth surface without holes. There are almost no impurities on the surface of the microcapsules (Figure 3(b)). Figure 3(c) shows a cracked microcapsule, which was prepared by simple vertical pressing using the SEM sample stage. It can be clearly seen that the formed microcapsules have an obvious shell-core structure with a very uniform thickness. All these findings indicated that the preparation method used in this study is suitable for the encapsulation of the phosphorescent microcapsules proposed in this study.

3.2. Microencapsulation. The FT-IR curves of phosphorescent liquid, PMMA, and ruptured and intact microcapsules are revealed in Figure 4. In the spectral curve of the phosphorescent liquid, the peak at 1650 cm^{-1} is due to the C=C stretching vibration, which was also found at ruptured microcapsules, which shows that the phosphorescent liquid was found inside the microcapsules. Combined with the absence of the 1650 cm^{-1} peak on intact microcapsules, the successful encapsulation of microcapsules was confirmed.

The chemical composition of the surface and core materials of the microcapsules can be studied through the EDS spectrum, as shown in Figure 5. Only C and O peaks are found on the surface of the microcapsule (Figure 5(a)), which is consistent with the chemical composition of PMMA. The Al and Sr elements belong to strontium aluminate. Al and Sr are not found on the surface of the microcapsules (Figure 5(b)), which also proves the successful encapsulation.

3.3. Size Distribution of Microcapsules. Figure 6 shows the particle size distribution of the phosphorescent microcapsules. The stirring speed of the fabrication process was set to five groups, which were 300 rpm, 500 rpm, 700 rpm, 900 rpm, and 1100 rpm. The results showed that the microcapsule cannot be successfully encapsulated under 300 rpm stirring. This may be because 300 rpm stirring cannot provide sufficient shear stress, which determines the low stability of the emulsion [33]. As a result, part of the core material could not be successfully encapsulated. Agglomeration also appeared among the successfully encapsulated microcapsules of 300 rpm after drying. It can be clearly seen from Figure 6(a) that the change in stirring rate greatly influences the particle size distribution of phosphorescent microcapsules. The microcapsules can be successfully fabricated and dried with a stirring speed of 500–1100 rpm. With the increase of stirring speed, the main diameter of microcapsules becomes smaller, and particle size distribution is narrow. This is due to the increase in stirring speed leading to an increase in shear force, which leads to a decrease in the size of the microcapsule particles. In the meantime, the viscosity of the emulsion is higher, and the emulsion is more stable. As shown in Figure 6(b), with the increase in stirring speed, the main diameter of microcapsules decreases, which can be used as a reference for preparing microcapsules of different sizes.

3.4. Analysis of Mechanical Properties. Microcapsule implantation's effect on the coating's mechanical properties is very important. In this section, the influence of composite microcapsules with different mass fractions (0.0wt %, 5.0wt%, 10wt%, and 15wt%) on microcapsule/epoxy resin composite coating was investigated by tensile strength test and compression strength test. The stress-strain curve of the tensile specimen is shown in Figure 7. The results show that with the increase of microcapsule concentration in microcapsule/epoxy resin composite coating, the fracture strength of microcapsule/epoxy resin composite coating increases first and then decreases. The breaking strength of epoxy resin coating without microcapsules is 36.14 MPa. The fracture strength of composite samples with a microcapsule content of 5% is 8.61% higher than that of epoxy resin without microcapsules. This is because when the microcapsule content is low, it can be dispersed in the coating without causing stress concentration. A small amount of the content of microcapsule can improve the toughness of the coating. It can be seen from Figure 7 that when the content of microcapsules continues to increase, the fracture strength of the microcapsule/epoxy resin composite coating containing 10wt% and 15wt% shows a decreasing trend compared with the coating without microcapsules, which decreases by 4.57% and 15.55%, respectively. This is mainly attributed to the poor dispersion and aggregation of microcapsules in the matrix as the filling amount of microcapsules increases. This phenomenon leads to stress concentration in the coating during the stress process, resulting in a decrease in the mechanical properties of the coating. In addition, the porosity and stress concentration of the coating increase due to the holes generated after the capsule rupture, which reduce the flexibility of the coating and accelerate the damage of the coating. Therefore, the coating containing 5% epoxy resin has the best tensile mechanical properties. Figure 8 shows the stress-strain curve of the compression test of samples with different contents of microcapsule at a strain rate of

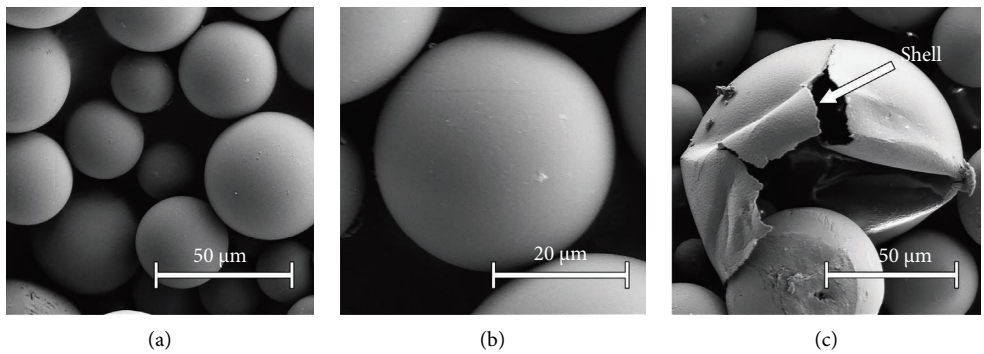

Figure 3: SEM images of microcapsules on (a) 2500 magnifications, (b) 6000 magnifications, and (c) ruptured microcapsule.

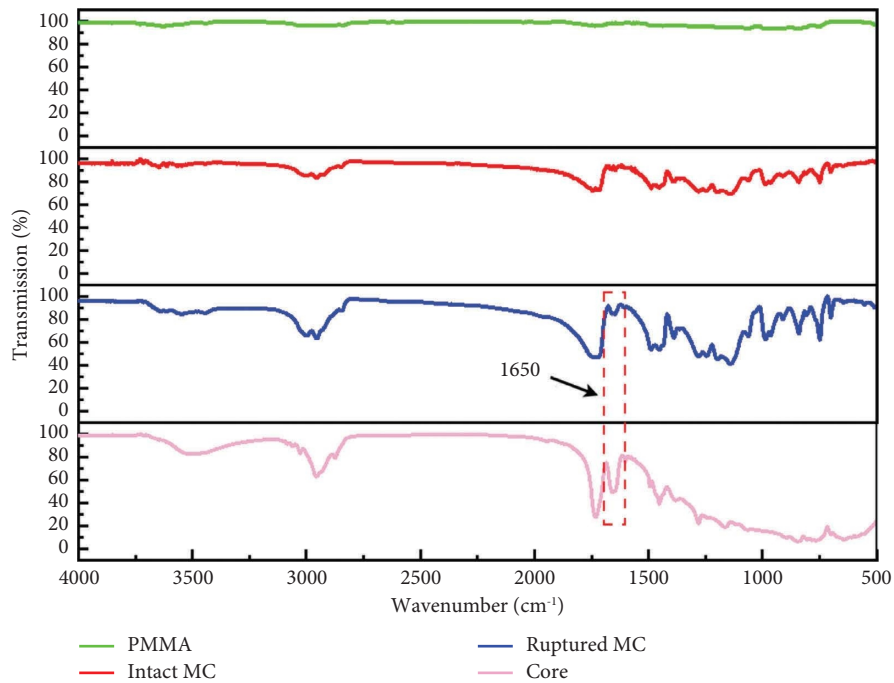

Figure 4: Infrared spectra of PMMA, intact microcapsules (MC), ruptured microcapsules, and phosphorescent liquid.

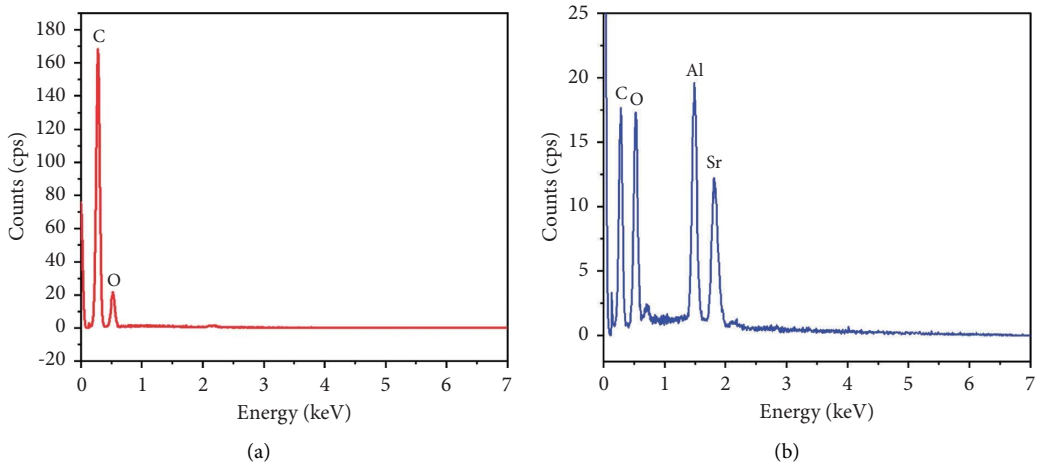

Figure 5: EDS spectra of (a) microcapsule and (b) phosphorescent liquid.

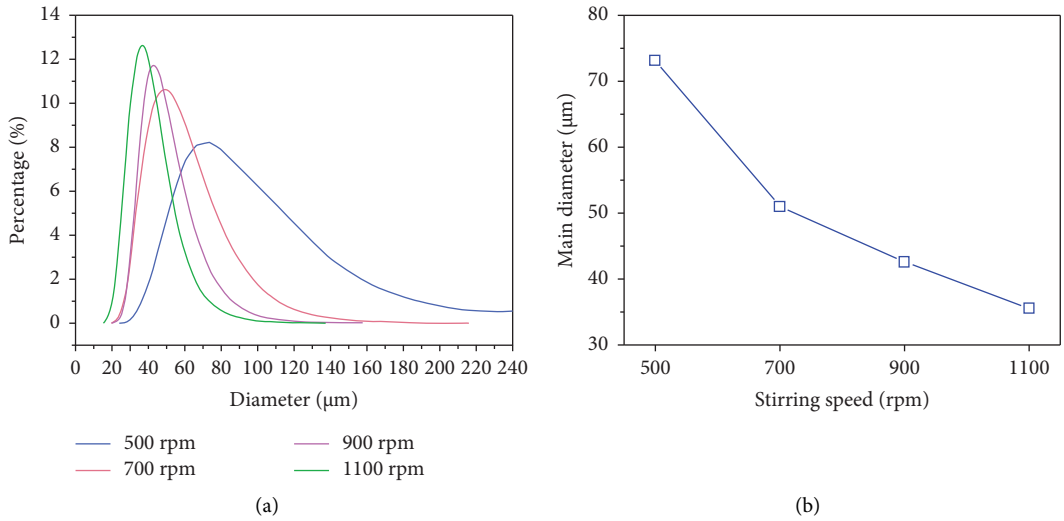

Figure 6: Particle size distribution of the phosphorescent microcapsules. (a) Effect of stirring speed on particle size distribution and (b) main diameter of the microcapsules.

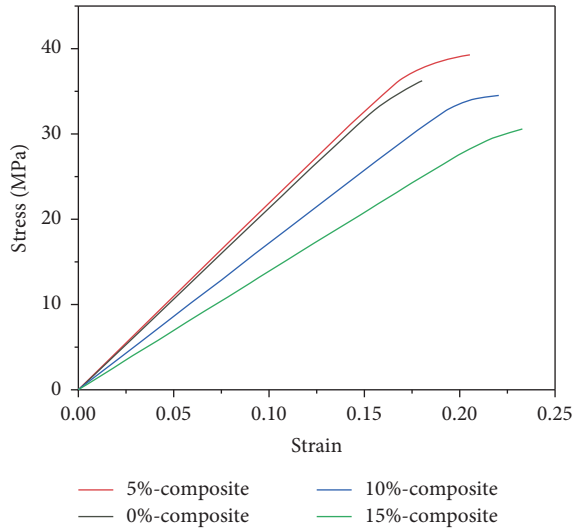

Figure 7: Stress-strain curve under tensile strength test of epoxy resin coating compounded with different mass fractions of microcapsules.

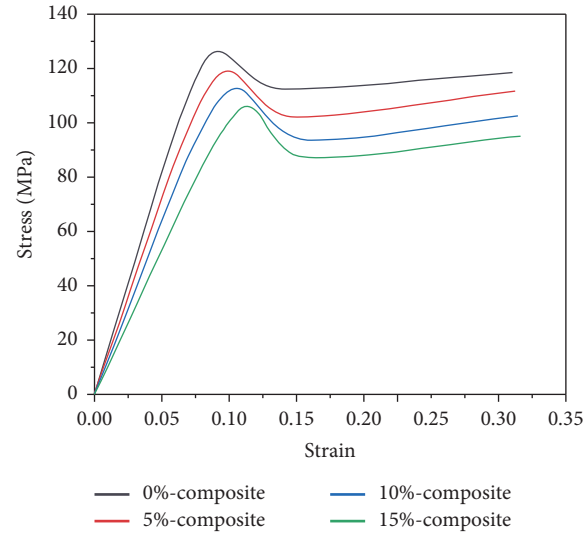

Figure 8: Stress-strain curve of epoxy resin coating compounded with different mass fractions of microcapsules under compression strength test.

$1000\,s^{-1}$. For all samples, a notable nonlinear region corresponding to the highest yield stress was seen following the initial linear region and the subsequent plastic flow process. The postyielding stress decline signifies strain softening, a characteristic often observed in ductile amorphous polymers. In all instances, plastic flow promptly followed strain softening and evident strain hardening. The maximum compressive stress is the smallest in the microcapsule/epoxy resin composite coating when the amount of microcapsules added is 15%. The maximum compressive stress of pure epoxy resin is the highest. When the contents of the microcapsule were 0.0wt%, 5.0wt%, 10wt%, and 15wt%, the peak stresses corresponding to the curves were 122.45 MPa, 115.37 MPa, 108.93 MPa, and 103.24 MPa, respectively. The dynamic yield strength of composite materials significantly decreases with the increase of microcapsule content. This is because agglomeration occurs when the content of microcapsules is high, leading to a decrease in the compressive strength of the composite material. On the other hand, the compressive strength of microcapsules is lower than that of epoxy resin. A large number of microcapsules break before the epoxy resin breaks when the composite material is subjected to external forces, leading to the destruction of the entire sample. Therefore, excessive microcapsule content is detrimental to the mechanical properties of the coating. Therefore, a microcapsule/epoxy resin composite coating with 5% microcapsule content and having good mechanical properties was selected as the coating for concrete crack sensing.

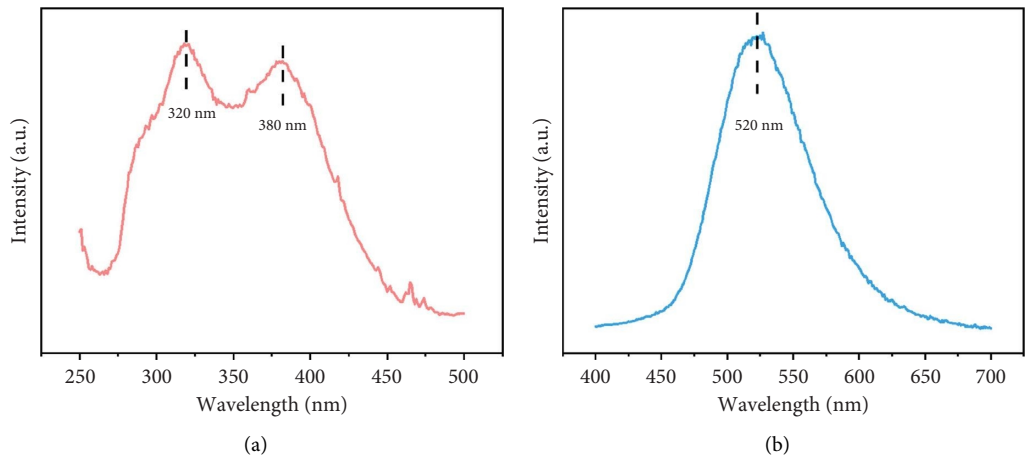

Figure 9: Phosphorescence spectra of microcapsules. (a) Excitation spectrum and (b) emission spectrum.

3.5. Evaluation of Phosphorescence Performance. The phosphorescence spectrum and excitation spectrum of microcapsules are shown in Figure 9. As shown in Figure 9(a), there are two phosphorescence peaks when the exciting wavelengths are 320 and 380 nm, respectively. Therefore, after being irradiated by UV rays with wavelengths of 320 nm and 380 nm, the highest brightness of the microcapsules can be excited. The phosphorescence intensity of the microcapsules was also characterized. As shown in Figure 9(b), the microcapsules have the strongest phosphorescence intensity at the wavelength of 520 nm.

3.6. Thermal Stability. The thermal stability of the microcapsules, phosphorescent liquid, and PMMA shell was characterized by TGA. Figure 10 shows the curves of the microcapsules, phosphorescent liquid, and PMMA shell mass loss. The phosphorescent liquid displays an obvious weight loss below 110°C. This is caused by the evaporation of the liquid in the phosphorescent liquid. The weight loss of the PMMA shell starts at 275°C, and the decomposition is finished at 400°C. After encapsulation, the curve of microcapsules shows no significant weight loss before 110°C. The weight of the microcapsules is decreased from 110°C. This is because the heat deflection temperature of the PMMA shell is reached [34], and part of the core material begins to leak. These findings suggest that the microencapsulation of phosphorescent liquid can significantly enhance the thermal stability.

The thermal stability of microcapsule phosphorescence performance is shown in Figure 11. Figure 11(a) shows the microcapsule phosphorescence performance after heating at different temperatures. There is no visible change in the phosphorescence effect of the microcapsules even after heating for 12 hours. Figure 11(b) shows the normal character of microcapsules. Microcapsules can maintain the initial dry powder state even if heated at 90°C for 12 hours. The microcapsules still have a strong phosphorescence performance at 110°C. However, because the heating temperature had reached the heat deflection temperature of PMMA, a certain bonding phenomenon appeared among the microcapsules, as shown in Figure 11(c). All these findings indicated that the microcapsules have a good working performance when the environment temperature is lower than 110°C.

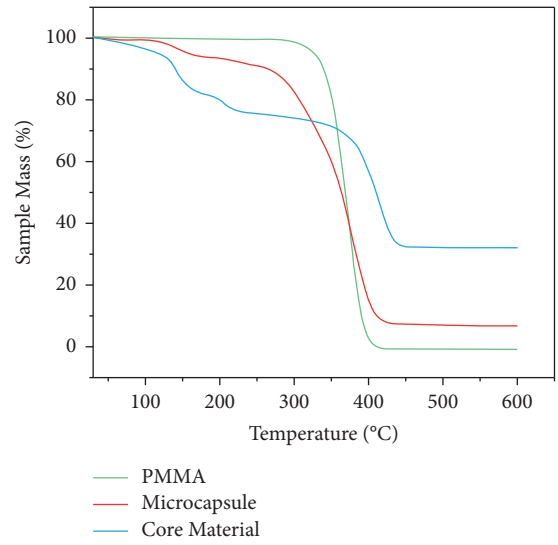

Figure 10: TGA curves of PMMA (green), phosphorescent microcapsule (red), and core material of microcapsule (blue).

3.7. Crack Sensing Test. Figure 12 shows the crack-sensing performance of microcapsules in conditions of different light and observation distances. The phosphorescent microcapsules containing coating was applied to the mortar sample's surface to evaluate the microcapsules' crack monitoring performance. A sharp blade was used to prepare a crack. After removing the excitation light source, all pictures were shot at 10°C. As shown in Figure 12(a), the crack width is about 0.25–0.5 mm and is not conspicuous under good lighting conditions before UV exposure. Figure 12(b) shows the performance of crack sensing after being excited by UV light in conditions of low light. The crack area emits clear green phosphorescence, which can be

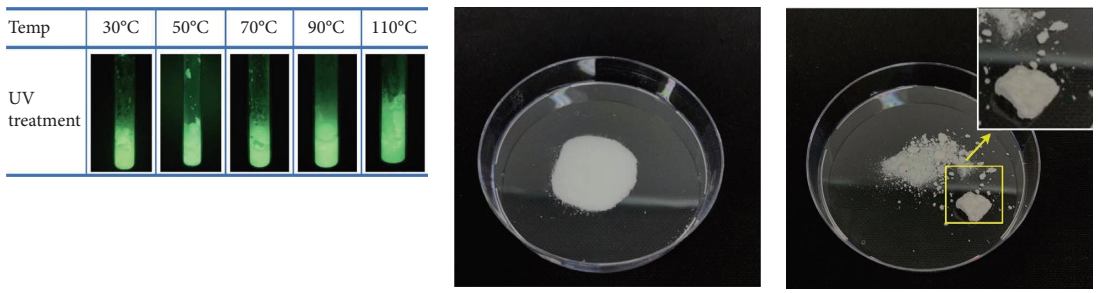

(a) (b) (c)

Figure 11: Thermal stability of microcapsule phosphorescent performance. (a) Phosphorescent performance of microcapsules after heating at different temperatures, (b) normal character of microcapsules, and (c) microcapsules heated to 110°C and bonded.

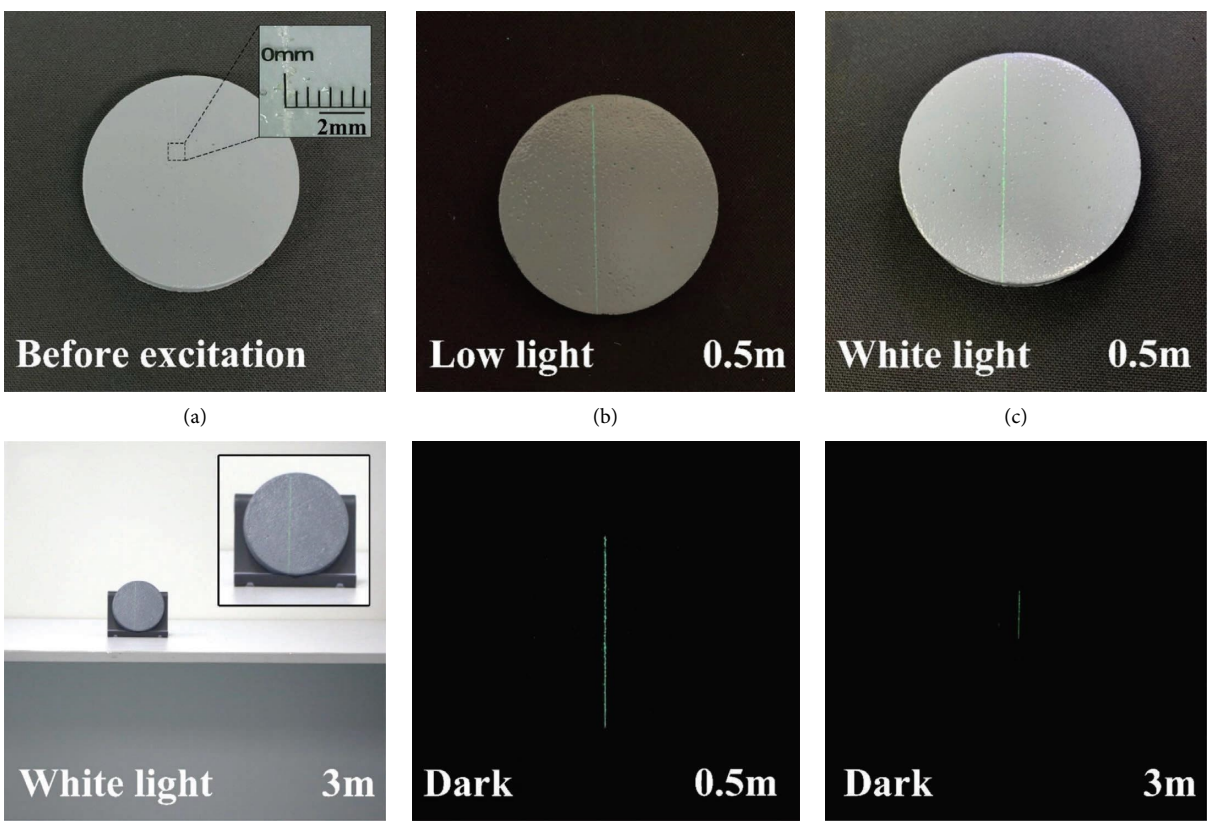

(a) (b) (c)

(d) (e) (f)

Figure 12: Crack report performance of microcapsules under different light conditions and observation distances. Photographs of crack (a) before excitation and after excitation in (b) low light environment at 50 cm, after excitation in the white light environment at (c) 50 cm and (d) 3 m, and after excitation in the environment at (e) 50 cm and (f) 3 m. All photos were taken after removing the excitation light source.

clearly observed in low-lighting conditions. The crack-sensing performance under good lighting conditions at distances of 0.5 m and 3 m are shown in Figures 12(c) and 12(d), respectively. Even at a distance of 3 m, the crack can be clearly captured by the naked eye. Figures 12(e) and 12(f) show the crack-sensing performance under dark conditions at distances of 0.5 m and 3 m. All these findings suggest that the phosphorescent microcapsules have good working performance under different light conditions. Even under good lighting conditions, inconspicuous cracks can be highlighted by phosphorescence making them observable with the naked eye. The duration of phosphorescence was also investigated. The coating before excitation is not visible in the darkness. After 10 seconds of excitation, the coating continuously emits green phosphorescence and slowly decays. After 10 minutes of observation, the phosphorescence of the coating is still visible to the naked eye. The characteristics of higher brightness and long-lasting make it possible to observe the crack without interference from the excitation light source.

4. Conclusions

A long-lasting phosphorescent microcapsule coating was proposed to detect cracks in concrete structures in this study. The microcapsules were successfully encapsulated by the solvent evaporation method. It was verified that the microcapsules were well-formed, and the stability of the core material could be effectively improved after encapsulating. The results of the excitation spectrum showed that after being irradiated by UV rays with wavelengths of 320 nm and 380 nm, the highest brightness of the microcapsules can be excited. The mechanical properties of microcapsules/epoxy resin composite coatings were studied, and the optimal content of microcapsules in the coating was determined to be 5%. The crack-sensing test showed that the fabricated microcapsules have obvious cracks indicating performance under different light conditions in the range of 10–90°C. After removing the excitation light source, the phosphorescent microcapsule could still provide more than 10 min luminescence for damage observation, which can effectively avoid the interference of the excitation light source and reduce the difficulty of crack observation. The proposed sensing material using long-lasting phosphorescent dye in this study may assist the further development of damage-sensing material applications in the field of structure monitoring.

Data Availability

Some or all data that support the findings of this study are available from the corresponding author upon request.

Conflicts of Interest

The authors declare that they have no conflicts of interest.

Acknowledgments

This work was supported by the Taishan Scholar Project of Shandong Province (No. TSHW20130956).

References

[1] D. Huang, Q. Zhang, and P. Qiao, "Damage and progressive failure of concrete structures using non-local peridynamic modeling," *Science China Technological Sciences*, vol. 54, no. 3, pp. 591–596, 2011.

[2] L. Chernin and D. V. Val, "Prediction of corrosion-induced cover cracking in reinforced concrete structures," *Construction and Building Materials*, vol. 25, no. 4, pp. 1854–1869, 2011.

[3] J. Ou and H. Li, "Structural Structural Health Monitoring in mainland China: Review and Future Trendsealth monitoring in mainland China: review and future trends," *Structural Health Monitoring*, vol. 9, no. 3, pp. 219–231, 2010.

[4] D. Zymelka and K. Togashi, "Carbon-based printed strain sensor array for remote and automated structural health monitoring," *Smart Materials and Structures*, vol. 29, no. 10, Article ID 105022, 2020.

[5] J. M. Lopez-Higuera, L. Rodriguez Cobo, A. Quintela Incera, and A. Cobo, "Fiber Fiber Optic Sensors in Structural Health Monitoringptic sensors in structural health monitoring," *Journal of Lightwave Technology*, vol. 29, no. 4, pp. 587–608, 2011.

[6] R. You, L. Ren, and G. Song, "A novel OFDR-based distributed optical fiber sensing tape: design, optimization, calibration and application," *Smart Materials and Structures*, vol. 29, no. 10, Article ID 105017, 2020.

[7] S. Villalba and J. R. Casas, "Application of optical fiber distributed sensing to health monitoring of concrete structures," *Mechanical Systems and Signal Processing*, vol. 39, no. 1-2, pp. 441–451, 2013.

[8] V. Agarwal, A. Shelke, B. Ahluwalia, F. Melandsø, T. Kundu, and A. Habib, "Damage localization in piezo-ceramic using ultrasonic waves excited by dual point contact excitation and detection scheme," *Ultrasonics*, vol. 108, Article ID 106113, 2020.

[9] H. Yu, L. Lu, P. Qiao, and Z. Wang, "Actuating and sensing mechanism of embedded piezoelectric transducers in concrete," *Smart Materials and Structures*, vol. 29, no. 8, Article ID 85020, 2020.

[10] Y. Ma, D. Yin, X. Wang, Y. Li, and Q. Jiang, "Cement-based piezoelectric composite sensor designed for charactering the three-dimensional stress state in concrete," *Smart Materials and Structures*, vol. 29, no. 8, Article ID 85048, 2020.

[11] C. Tuloup, W. Harizi, Z. Aboura, and Y. Meyer, "Structural health monitoring of polymer-matrix composite using embedded piezoelectric ceramic transducers during several four-points bending tests," *Smart Materials and Structures*, vol. 29, no. 12, Article ID 125011, 2020.

[12] J. Luan, Q. Wang, X. Zheng, and Y. Li, "Flexible strain sensor with good durability and anti-corrosion property based on metal/polymer composite films embedded with silver nanowires," *Archives of Civil and Mechanical Engineering*, vol. 20, no. 4, p. 133, 2020.

[13] A. Nair and C. S. Cai, "Acoustic emission monitoring of bridges: Acoustic emission monitoring of bridges: Review and case studieseview and case studies," *Engineering Structures*, vol. 32, no. 6, pp. 1704–1714, 2010.

[14] S. Cantero-Chinchilla, J. L. Beck, M. J. Chiachío, D. Chronopoulos, and A. L. Jones, "Optimal sensor and actuator placement for structural health monitoring via an efficient convex cost-benefit optimization," *Mechanical Systems and Signal Processing*, vol. 144, Article ID 106901, 2020.

[15] T N. Tallman, D. J. N. Smyl, and D. J. Smyl, "Structural health and condition monitoring via electrical impedance tomography in self-sensing materials: a review," *Smart Materials and Structures*, vol. 29, no. 12, Article ID 123001, 2020.

[16] O. Rifaie-Graham, E. A. Apebende, L K. Bast, and N. Bruns, "Self-Reporting Self-Reporting Fiber-Reinforced Composites That Mimic the Ability of Biological Materials to Sense and Report Damageiber-reinforced composites that mimic the ability of biological materials to sense and report damage," *Advanced Materials*, vol. 30, no. 19, Article ID 1705483, 2018.

[17] R. Zhang, Q. Wang, and X. Zheng, "Flexible mechanochromic photonic crystals: routes to visual sensors and their mechanical properties," *Journal of Materials Chemistry C*, vol. 6, no. 13, pp. 3182–3199, 2018.

[18] X. Zheng, Q. Wang, J. Luan et al., "Angle-dependent structural colors in a nanoscale-grating photonic crystal fabricated by reverse nanoimprint technology," *Beilstein Journal of Nanotechnology*, vol. 10, pp. 1211–1216, 2019.

[19] S. Kling and T. Czigány, "Damage detection and self-repair in hollow glass fiber fabric-reinforced epoxy composites via fiber

filling," *Composites Science and Technology*, vol. 99, pp. 82–88, 2014.

[20] S. Zainuddin, T. Arefin, A. Fahim et al., "Recovery and improvement in low-velocity impact properties of e-glass/epoxy composites through novel self-healing technique," *Composite Structures*, vol. 108, pp. 277–286, 2014.

[21] X. Zheng, Q. Wang, Y. Li, J. Luan, N. Wang, and L. Li, "Microcapsule-Microcapsule-Based Visualization Smart Sensors for Damage Detection: Principles and Applicationsased visualization smart sensors for damage detection: principles and applications," *Advanced Materials Technologies*, vol. 5, no. 2, Article ID 1900832, 2020.

[22] C. Calvino and C. Weder, "Microcapsule-Microcapsule-Containing Self-Reporting Polymersontaining self-reporting polymers," *Small*, vol. 14, no. 46, Article ID 1802489, 2018.

[23] W. Li, C. C. Matthews, K. Yang et al., "Autonomous Autonomous Indication of Mechanical Damage in Polymeric Coatingsndication of mechanical damage in polymeric coatings," *Advanced Materials*, vol. 28, no. 11, pp. 2189–2194, 2016.

[24] M. Hu, S. Peil, Y. Xing et al., "Monitoring crack appearance and healing in coatings with damage self-reporting nanocapsules," *Materials Horizons*, vol. 5, no. 1, pp. 51–58, 2018.

[25] B. Di Credico, G. Griffini, M. Levi, and S. Turri, "Microencapsulation of a UV-Microencapsulation of a UV-Responsive Photochromic Dye by Means of Novel UV-Screening Polyurea-Based Shells for Smart Coating Applicationsesponsive photochromic dye by means of novel UV-screening polyurea-based shells for smart coating applications," *ACS Applied Materials & Interfaces*, vol. 5, no. 14, pp. 6628–6634, 2013.

[26] X. Zheng, Q. Wang, Y. Li, S. Xu, and Y. Li, "Fabrication of self-reactive microcapsules as color visual sensing for damage reporting," *Journal of Materials Science*, vol. 55, no. 21, pp. 8861–8867, 2020.

[27] Y. Li, Q. Wang, X. Zheng, Y. Li, and J. Luan, "Microcapsule encapsulated with leuco dye as a visual sensor for concrete damage indicationviacolor variation," *RSC Advances*, vol. 10, no. 3, pp. 1226–1231, 2020.

[28] Y. K. Song, K. H. Lee, D. M. Kim, and C. M. Chung, "A microcapsule-type fluorescent probe for the detection of microcracks in cementitious materials," *Sensors and Actuators B: Chemical*, vol. 222, pp. 1159–1165, 2016.

[29] Y K. Song, B. Kim, T. H. Lee et al., "Fluorescence Fluorescence Detection of Microcapsule-Type Self-Healing, Based on Aggregation-Induced Emissionetection of microcapsule-type self-healing, based on aggregation-induced emission," *Macromolecular Rapid Communications*, vol. 38, no. 6, Article ID 1600657, 2017.

[30] J. Liu, J. Feng, Y. Yu et al., "Fabrication of a Fabrication of a Luminescent Supramolecular Hydrogel Based on the AIE Strategy of Gold Nanoclusters and their Application as a Luminescence Switchuminescent supramolecular hydrogel based on the AIE strategy of gold nanoclusters and their application as a luminescence switch," *The Journal of Physical Chemistry C*, vol. 124, no. 43, pp. 23844–23851, 2020.

[31] J. Nance and T. D. Sparks, "Comparison of coatings for SrAl2O4:Eu2+,Dy3+ powder in waterborne road striping paint under wet conditions," *Progress in Organic Coatings*, vol. 144, Article ID 105637, 2020.

[32] J. Nance and T. D. Sparks, "From streetlights to phosphors: From streetlights to phosphors: A review on the visibility of roadway markings review on the visibility of roadway markings," *Progress in Organic Coatings*, vol. 148, Article ID 105749, 2020.

[33] R. Yulianingsih and S. Gohtani, "The influence of stirring speed and type of oil on the performance of pregelatinized waxy rice starch emulsifier in stabilizing oil-in-water emulsions," *Journal of Food Engineering*, vol. 280, Article ID 109920, 2020.

[34] B. Tang, T. Lin, C. Wu, and S. Zhang, "Heat-resistant PMMA photonic crystal films with bright structural color," *Dyes and Pigments*, vol. 99, no. 3, pp. 1022–1028, 2013.